Pulsed EM Field Response of a Thin, High-Contrast, Finely Layered Structure With Dielectric and Conductive Properties

Adrianus T. de Hoop, *Member, IEEE*, and Lijun Jiang, *Member, IEEE*

***Abstract*—The response of a thin, high-contrast, finely layered structure with dielectric and conductive properties to an incident, pulsed, electromagnetic field is investigated theoretically. The fine layering causes the standard spatial discretization techniques to solve Maxwell's equations numerically to be practically inapplicable. To overcome this difficulty, an approximate method is proposed that models the interaction of the layer with an incident electromagnetic field via a boundary condition that expresses the in-plane conduction and contrast electric polarization currents in terms of the exciting incident field by relating the jump in the tangential component of the magnetic field strength across the layer in terms of the (continuous) tangential component of the electric field strength in the layer. In the pertaining layer admittance coefficient, the integrated values of the conductance and the contrast permittivity profiles across the layer occur. The model is applied to the scattering of an incident plane wave with pulsed time signature by a layer of infinite extent. Expressions for pulse shapes of the scattered field are obtained. In them, the layer properties and the direction of incidence and polarization of the incident wave occur as parameters. Numerical results are presented for reflected and transmitted wave pulse shapes for some parameter values.**

***Index Terms*—High-contrast thin layers, pulsed EM fields.**

I. Introduction

THIN layered structures with electromagnetic (EM) properties that appreciably differ from those of their surroundings are encountered in diverse areas of electronics engineering. Examples are: aircraft antenna radomes, micro- and nano-electronic devices and integrated optical devices. In the analysis, design and optimizations stages of all these technical applications, as well as their associated electromagnetic interference analyses, the computational modeling of the governing electromagnetic field is a subject of considerable importance and concern. Standard approaches to the discretization of Maxwell's equations in such structures are faced with serious difficulties as to the meshing or gridding of the configuration [1]. To overcome this difficulty, several approximate procedures have been proposed. They are all of a physically heuristic nature and their degree of accuracy and usefulness requires testing against the results of certain benchmark configurations.

As to the heuristic approaches one can, broadly speaking, distinguish three different kinds of reasoning. In [2], the contrast volume source type electromagnetic field representations with the Green's functions (propagators) of the homogeneous, isotropic embedding (usually free space) serve as the point of departure. By a judicious reasoning, the pertaining thin layers of contrast volume electric and magnetic current are replaced with their corresponding equivalent surface currents. In [3], the frequency-domain counterpart of the Lorentz reciprocity relation of the time-convolution type [4, Sec. 28.2] is alternatively applied to the interior of the layer and the exterior of the layer, under the use of field reaction concept introduced by Rumsey [5] and the field equivalence theorem [6, Ch. 30]. These two approaches are of the global type in that they employ field representations or theorems that apply to the configuration space as a whole to arrive at more or less local interface jump conditions across the layer. Such local conditions can, however, also be constructed directly from local arguments applied to Maxwell's equations. This third kind of approach is followed by Collin [7, p. 693] and by Senior [8]. A fourth kind of approach goes via the use of surface integral equations [1]. An overview of the different approaches, as well as their application to a number of canonical problems, can be found in [9].

In the present paper we employ a kind of local approach that was introduced by Schoenberg and Muir [10] in the context of elastodynamic wave propagation in finely layered rock formations and that has also been applied to acoustic wave propagation [11]. The procedure leads to local jump conditions on the tangential components of the electric and/or magnetic field strengths across the layer, the coefficients in which can be interpreted as local Kirchhoff lumped electric circuit elements (such as conductance and capacitance for a conductive and dielectric layer), whose values are representative for the field transfer in the direction normal to the layer.

Until now, the literature on the subject is concentrated on the frequency-domain analysis of the electromagnetic fields involved. Nowadays, a substantial range of applications employs pulsed EM fields. For this reason, we concentrate on the direct time-domain analysis of the problem and correspondingly use some auxiliary tools from linear, time-invariant, causal system's theory, amongst which the time Laplace transformation properties of causal signals. The configuration that we consider is a thin, finely layered, high-contrast, planar sheet with electrically conductive and dielectric properties that differ from the ones of the surrounding medium. A local application of Maxwell's

Manuscript received January 21, 2008; revised October 06, 2008. First published May 02, 2009; current version published August 05, 2009.

A. T. de Hoop is with the Laboratory of Electromagnetic Research, Faculty of Electrical Engineering, Mathematics and Computer Science, Delft University of Technology, 2628 CD Delft, The Netherlands (e-mail: a.t.dehoop@tudelft.nl).

L. Jiang is with the IBM T. J. Watson Research Center, Yorktown Heights, NY 10598 USA (e-mail: ljiang@us.ibm.com).

Color versions of one or more of the figures in this paper are available online at http://ieeexplore.ieee.org.

Digital Object Identifier 10.1109/TAP.2009.2021877

equations in integral form (circulation and flux integrals) provide the interface jump conditions we are after (Section II). In the conditions, the local equivalent layer conductance and the local equivalent layer capacitance occur. To show what response such a configuration produces on a pulsed incident EM field, we present results for the reflection and transmission of a plane wave incident on a uniform layer of infinite extent with highly contrasting conductive and dielectric properties (Section III). Expressions for the pulse shapes of the reflected and transmitted fields are obtained. In them, the layer properties and the direction of incidence and state of polarization of the incident wave (electric field parallel to the layer or magnetic field parallel to the layer) occur as parameters. Numerical results for some parameter values are shown in Section IV. To arrive at the results, Matlab7.1 routines have been composed that, after properly editing the input data, generate a variety of field time snaps at a specified location, Matlab "images" (2D color density plots) of the field distribution in space at successive time instants (animation) and Matlab "quivers" (2D vector plots) of the Poynting vector distribution in space at successive time instants (animation).[1] Section V contains conclusions.

In Lomakin, V., Steinberg, B. Z. and Heyman, E. [12] the multiresolution homogenization method is used to arrive at an effective-medium theory for the interaction of incident pulsed EM fields with a finely layered laminate. The method is based upon subdividing the inhomogeneity across the layer into a successively finer distribution of sublayers (via a kind of wavelet decomposition) and solving the resulting spectral- domain one-dimensional time-domain field equations for the relevant E- and H-polarized field constituents. Nowhere in the analysis is it necessary to assume that the contrast in the layer with repsect to its embedding is large (although that case is included in the analysis). The multiresolution homogenization method allows one to judge, at each scale of fineness, whether this scale suffices to handle the interaction with a pulsed incident field, given the latter's pulse time width. Our method is far more elementary: it is based on (the integral-form of) Maxwell's field equations, yields a simple approximate interface boundary condition for large contrasts based on an asymptotic order concept, but it lacks the possibility for refinement if the degree of approximation turns out to be insufficient. In this respect, the method of Lomakin, V., Steinberg, B.Z. and Heyman, E. more basically and more generally handles the problem of pulsed field interaction with finely layered laminates, but at the cost of a substantially more elaborate and extensive mathematical apparatus.

The impetus for the research arose in the context of the computational investigation into the signal integrity of electromagnetic fields in thin layered microelectronic structures. In the near future, the pulse time widths of operation in such devices attain values where a description of the behavior in terms of Kirchhoff lumped electric circuit elements is beyond its range of applicability and a full Maxwell field analysis is a necessity. The applicability of the approximation lies in the range where the parameter: (thickness of the layer) / (electromagnetic wavespeed $\times$ incident wave pulse time width) is small.

[1]A copy of the routines is available upon request from the first author at: a.t.dehoop@tudelft.nl

II. Formulation of the Problem and Derivation of the Thin-Layer, High-Contrast, Boundary Condition

Position in the configuration is specified through the Cartesian coordinates $\{x, y, z\}$ with respect to an orthogonal Cartesian reference frame with the origin $\mathcal{O}$ and the three mutually perpendicular base vectors $\{\boldsymbol{i}_x, \boldsymbol{i}_y, \boldsymbol{i}_z\}$ of unit length each. In the indicated order, the base vectors form a right-handed system. The vectorial position is denoted by $\boldsymbol{r} = x\boldsymbol{i}_x + y\boldsymbol{i}_y + z\boldsymbol{i}_z$. The time coordinate is t. The high-contrast, layered specimen occupies the domain

$$\mathcal{D} = \left\{(x, y) \in \Sigma \subset \mathbb{R}^2, -\frac{d}{2} < z < \frac{d}{2}\right\} \tag{1}$$

where $d > 0$ is the thickness of the layer and Σ is its spatial support in the (x, y)-plane. The background medium occupies the entire $\mathbb{R}^3$. Somewhere in this medium, sources generate an incident electromagnetic field. This field is scattered by the contrasting specimen (Fig. 1). The background medium is taken to be lossless, homogeneous and isotropic with electric permittivity ϵ_0 and magnetic permeability μ_0. The electromagnetic properties of the layer are characterized by its electric conductivity $\sigma(\boldsymbol{r})$ and its electric permittivity $\epsilon(\boldsymbol{r})$; its magnetic permeability μ_0 is taken to be the same as the one of the background medium. We assume the travel time of the incident wave across the layer to be negligible with respect to the time width of the incident pulse. Furthermore, the electric properties of the layered material, i.e., its electric conductivity and/or its electric permittivity are assumed to be so high that the quantities

$$G_{\mathrm{L}} = \int_{z=-d/2}^{d/2} \sigma(\boldsymbol{r}) \mathrm{d}z \tag{2}$$

and

$$C_{\mathrm{L}} = \int_{z=-d/2}^{d/2} \epsilon(\boldsymbol{r}) \mathrm{d}z \tag{3}$$

are of order $O(1)$ as $d \downarrow 0$. (Note that G_{L} has the dimension of a conductance and C_{L} has the dimension of a capacitance.) Let $\boldsymbol{E}(\boldsymbol{r}, t)$ denote the electric field strength and $\boldsymbol{H}(\boldsymbol{r}, t)$ the magnetic field strength. Then, for any source-free bounded subdomain of the configuration $\Omega \subset \mathbb{R}^3$, with closed boundary surface $\partial\Omega$ with piecewise continuous unit vector $\boldsymbol{\nu}$ along its outward normal, the field quantities satisfy the volume integrated Maxwell equations

$$\int_{\partial\Omega} \boldsymbol{\nu} \times \boldsymbol{H} \mathrm{d}A = \int_{\Omega} (\epsilon \partial_t \boldsymbol{E} + \sigma \boldsymbol{E}) \mathrm{d}V \tag{4}$$

$$\int_{\partial\Omega} \boldsymbol{\nu} \times \boldsymbol{E} \mathrm{d}A = -\int_{\Omega} \mu_0 \partial_t \boldsymbol{H} \mathrm{d}V. \tag{5}$$

Then, since all field components are bounded inside and outside the layer, the application of (5) to a "pillbox" perpendicularly crossing the layer, leads to

$$\boldsymbol{i}_z \times \boldsymbol{E}\left(x, y, \frac{d}{2}, t\right) - \boldsymbol{i}_z \times \boldsymbol{E}\left(x, y, -\frac{d}{2}, t\right) = O(d) \text{ for } (x, y) \in \Sigma \text{ as } d \downarrow 0. \tag{6}$$

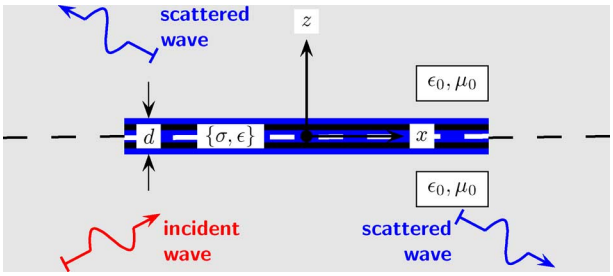

Fig. 1. Configuration with thin, finely layered, high-contrast structure in a homogeneous, isotropic background medium, with incident and scattered EM waves.

Similarly, the application of (4) to a "pillbox" perpendicularly crossing the layer, leads, taking into account (2), (3) and (6), to

$$\boldsymbol{i}_z \times \boldsymbol{H}\left(x, y, \frac{d}{2}, t\right) - \boldsymbol{i}_z \times \boldsymbol{H}\left(x, y, -\frac{d}{2}, t\right) = (G_{\mathrm{L}} + C_{\mathrm{L}}\partial_t)\boldsymbol{E}(x, y, 0, t) + O(d) \text{ for } (x, y) \in \Sigma \text{ as } d \downarrow 0. \quad (7)$$

With $\{\boldsymbol{E}^{\mathrm{i}}, \boldsymbol{H}^{(\mathrm{i}}\}(\boldsymbol{r}, t)$ as the *incident* field (i.e., the field in the absence of the scattering specimen), the field $\{\boldsymbol{E}^{\mathrm{s}}, \boldsymbol{H}^{\mathrm{s}}\}(\boldsymbol{r}, t)$ *scattered* by the structure is

$$\begin{aligned} \boldsymbol{E}^{\mathrm{s}}(\boldsymbol{r}, t) &= \boldsymbol{E}(\boldsymbol{r}, t) - \boldsymbol{E}^{\mathrm{i}}(\boldsymbol{r}, t), \\ \boldsymbol{H}^{\mathrm{s}}(\boldsymbol{r}, t) &= \boldsymbol{H}(\boldsymbol{r}, t) - \boldsymbol{H}^{\mathrm{i}}(\boldsymbol{r}, t) \\ &\text{for } \boldsymbol{r} \in \mathbb{R}^3. \end{aligned} \quad (8)$$

The scattered field is causally related to the action of the volume source density of *electric contrast current* $\boldsymbol{J}^{\mathrm{s}}$ via the volume integrated Maxwell equations [cf. (4) – (5)]

$$\int_{\partial\Omega} \boldsymbol{\nu}^{\mathrm{out}} \times \boldsymbol{H}^{\mathrm{s}} \mathrm{d}A = \int_{\Omega} \epsilon_0 \partial_t \boldsymbol{E}^{\mathrm{s}} \mathrm{d}V + \int_{\mathcal{D}} \boldsymbol{J}^{\mathrm{s}} \mathrm{d}V \quad (9)$$

$$\int_{\partial\Omega} \boldsymbol{\nu}^{\mathrm{out}} \times \boldsymbol{E}^{\mathrm{s}} \mathrm{d}A = -\int_{\Omega} \mu_0 \partial_t \boldsymbol{H}^{\mathrm{s}} \mathrm{d}V \quad (10)$$

in which

$$\boldsymbol{J}^{\mathrm{s}} = (\epsilon - \epsilon_0)\partial_t \boldsymbol{E} + \sigma \boldsymbol{E} \text{ with } \mathrm{supp}\,(\boldsymbol{J}^{\mathrm{s}}) = \mathcal{D}. \quad (11)$$

Carrying out the integration with respect to z in the integral containing $\boldsymbol{J}^{\mathrm{s}}$ in the right-hand side of (9) and using (2) and (3), we obtain the contrast sheet electric current density

$$\boldsymbol{J}^{\mathrm{s}}_{\mathrm{sheet}} = (G_{\mathrm{L}} + C_{\mathrm{L}}\partial_t)\boldsymbol{E}(x, y, 0, t) \text{ for } (x, y) \subset \Sigma. \quad (12)$$

Proceeding with (9) and (10) as with (4) and (5), we obtain the boundary conditions for the scattered field as

$$\boldsymbol{i}_z \times \boldsymbol{E}^{\mathrm{s}}\left(x, y, \frac{d}{2}, t\right) - \boldsymbol{i}_z \times \boldsymbol{E}^{\mathrm{s}}\left(x, y, -\frac{d}{2}, t\right) = O(d) \text{ for } (x, y) \in \Sigma \text{ as } d \downarrow 0 \quad (13)$$

and

$$\boldsymbol{i}_z \times \boldsymbol{H}^{\mathrm{s}}\left(x, y, \frac{d}{2}, t\right) - \boldsymbol{i}_z \times \boldsymbol{H}^{\mathrm{s}}\left(x, y, -\frac{d}{2}, t\right) = \boldsymbol{J}^{\mathrm{s}}_{\mathrm{sheet}} + O(d) \text{ for } (x, y) \in \Sigma \text{ as } d \downarrow 0. \quad (14)$$

Equations (13) and (14) are compatible with (6) and (7), respectively, since the incident field is continuous across the layer.

From (14) it is evident that $\boldsymbol{i}_z \cdot \boldsymbol{J}^{\mathrm{s}}_{\mathrm{sheet}} = 0$, i.e., $\boldsymbol{J}^{\mathrm{s}}_{\mathrm{sheet}}$ has only non-zero components in the plane of the layer. This has the consequence that the scattered field has class "even" symmetry with respect to the plane $\{z = 0\}$, i.e., ([4, Sec. 18.5])

$$\{E^{\mathrm{s}}_x, E^{\mathrm{s}}_y, H^{\mathrm{s}}_z\}(x, y, -z, t) = \{E^{\mathrm{s}}_x, E^{\mathrm{s}}_y, H^{\mathrm{s}}_z\}(x, y, z, t) \text{ for all } \boldsymbol{r} \in \mathbb{R}^3 \quad (15)$$

$$\{E^{\mathrm{s}}_z, H^{\mathrm{s}}_x, H^{\mathrm{s}}_y\}(x, y, -z, t) = -\{E^{\mathrm{s}}_z, H^{\mathrm{s}}_x, H^{\mathrm{s}}_y\}(x, y, z, t) \text{ for all } \boldsymbol{r} \in \mathbb{R}^3. \quad (16)$$

In any computational procedure, this feature reduces the overall computation time. Although our procedure employing the volume integrated Maxwell equations to arrive at the saltus-type field boundary conditions across the layer is straightforward, the conditions could also have been obtained via the standard (circulation and flux) integral form of the source free field equations:

$$\oint_{\mathcal{C}} \boldsymbol{H}^{\mathrm{s}} \cdot \boldsymbol{\tau} \mathrm{d}s = \int_{\mathcal{S}} (\epsilon_0 \partial_t \boldsymbol{E}^{\mathrm{s}} + \boldsymbol{J}^{\mathrm{s}}) \cdot \boldsymbol{\nu} \mathrm{d}A \quad (17)$$

$$\oint_{\mathcal{C}} \boldsymbol{E}^{\mathrm{s}} \cdot \boldsymbol{\tau} \mathrm{d}s = -\int_{\mathcal{S}} \mu_0 \partial_t \boldsymbol{H}^{\mathrm{s}} \cdot \boldsymbol{\nu} \mathrm{d}A \quad (18)$$

where $\mathcal{S}$ is any bounded, two-sided surface, with unit vector $\boldsymbol{\nu}$ along its normal, $\mathcal{C}$ is the oriented boundary curve of $\mathcal{S}$, with unit vector $\boldsymbol{\tau}$ along its tangent (with the condition that $\boldsymbol{\nu}$ and $\boldsymbol{\tau}$ form a right-handed system). These latter equations entail the *EM compatibility relations*

$$\int_{\text{closed surface}} (\epsilon_0 \partial_t \boldsymbol{E}^{\mathrm{s}} + \boldsymbol{J}^{\mathrm{s}}) \cdot \boldsymbol{\nu}^{\mathrm{out}} \mathrm{d}A = 0 \quad (19)$$

$$\int_{\text{closed surface}} \mu_0 \partial_t \boldsymbol{H}\mathrm{s} \cdot \boldsymbol{\nu}^{\mathrm{out}} \mathrm{d}A = 0 \quad (20)$$

for any closed surface with sourcefree interior and outward unit vector along its normal $\boldsymbol{\nu}^{\mathrm{out}}$. Of these, (19) leads, upon application to a "pillbox" perpendicularly crossing the side surface of the layer, taking into account that $\boldsymbol{J}^{\mathrm{s}}$ vanishes outside $\mathcal{D}$ and integrating the result with respect to z to

$$\boldsymbol{\nu}_{\Sigma} \cdot \boldsymbol{J}^{\mathrm{s}}_{\mathrm{sheet}} = 0 \text{ for } (x, y) \in \partial\Sigma \quad (21)$$

i.e., along the rim $\partial\Sigma$ of Σ the contrast sheet electric current runs parallel to the rim. The incorporation of this "edge condition" into any computational procedure is of paramount importance, since the violation of it leads to field quantities with a too high singularity at the rim, as a consequence of which the uniqueness of field as specified by field equations + boundary conditions + initial conditions can no longer be guaranteed [13]–[16].

To illustrate a number of properties of the field scattered by the structure, we consider in Section III the case of a plane, pulsed, incident wave propagating in the (x, z)-plane, by a thin, high-contrast layer of infinite extent.

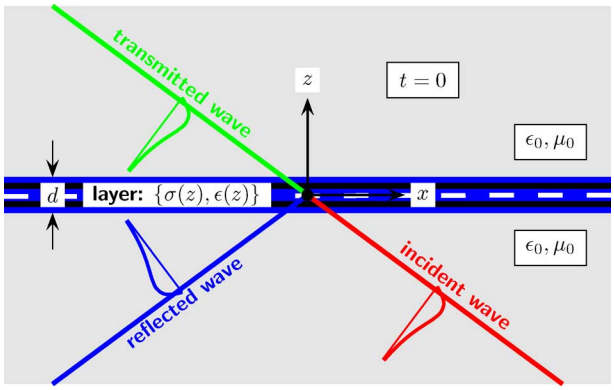

Fig. 2. Configuration with finely layered, high-contrast layer of infinite extent, with incident, reflected and transmitted pulsed EM waves.

III. Plane-Wave Reflection Against and Transmission Across a Thin, High-Contrast Layer of Infinite Extent

The thin, high-contrast layer of infinite extent occupies the plane $\{z = 0\}$. In the domain

$$\mathcal{D}^- = \{(x, y) \in \mathbb{R}^2, -\infty < z < 0\} \tag{22}$$

an incident plane wave is generated; in this domain reflection against the layer takes place. In the domain

$$\mathcal{D}^+ = \{(x, y) \in \mathbb{R}^2, 0 < z < \infty\} \tag{23}$$

transmission across the layer takes place (Fig. 2). The incident wave is taken to propagate in the (x, z)-plane which makes all field components independent of y. In view of this property, the electromagnetic field in the configuration decomposes into an E-polarized field with the electric field parallel to the layer and an H-polarized field with the magnetic field parallel to the layer. Then, using the scattering description discussed in Section II, taking into account the symmetry properties (15) and (16) and denoting by $\boldsymbol{\alpha} = \alpha_x \boldsymbol{i}_x + \alpha_z \boldsymbol{i}_z$, with $\alpha_x^2 + \alpha_z^2 = 1$, the unit vector in the direction of propagation of the incident wave, the representations for the field components can be written as:

A. E-Polarized Field

$$\{H_x^{\mathrm{i}}, E_y^{\mathrm{i}}, H_z^{\mathrm{i}}\} = \{-\alpha_z Y_0, 1, \alpha_x Y_0\} \times E_0^{\mathrm{i}}\left[t - \frac{(\alpha_x x + \alpha_z z)}{c_0}\right] \text{ for } \boldsymbol{r} \in \mathbb{R}^3 \tag{24}$$

$$\{H_x^{\mathrm{s}}, E_y^{\mathrm{s}}, H_z^{\mathrm{s}}\} = \{\mp\alpha_z Y_0, 1, \alpha_x Y_0\} \times E_0^{\mathrm{s}}\left[t - \frac{(\alpha_x x \pm \alpha_z z)}{c_0}\right] \text{ for } \boldsymbol{r} \in \mathcal{D}^{\pm} \tag{25}$$

where $c_0 = (\epsilon_0 \mu_0)^{-1/2}$ is the electromagnetic wave speed in the background medium, $Y_0 = (\epsilon_0/\mu_0)^{1/2}$ is the plane-wave admittance of the medium, $E_0^{\mathrm{i}}(t)$ is the signature of the incident E-polarized pulse, $E_0^{\mathrm{s}}(t)$ is the signature of the scattered E-polarized pulse, and

B. H-Polarized Field

$$\{E_x^{\mathrm{i}}, H_y^{\mathrm{i}}, E_z^{\mathrm{i}}\} = \{\alpha_z Z_0, 1, -\alpha_x Z_0\} \times H_0^{\mathrm{i}}\left[t - \frac{(\alpha_x x + \alpha_z z)}{c_0}\right] \text{ for } \boldsymbol{r} \in \mathbb{R}^3 \tag{26}$$

$$\{E_x^{\mathrm{s}}, H_y^{\mathrm{s}}, E_z^{\mathrm{s}}\} = \pm\{\pm\alpha_z Z_0, 1, -\alpha_x Z_0\} \times H_0^{\mathrm{s}}\left[t - \frac{(\alpha_x x \pm \alpha_z z)}{c_0}\right] \text{ for } \boldsymbol{r} \in \mathcal{D}^{\pm} \tag{27}$$

where $Z_0 = (\mu_0/\epsilon_0)^{1/2}$ is the plane-wave impedance of the medium, $H_0^{\mathrm{i}}(t)$ is the signature of the incident H-polarized pulse and is $H_0^{\mathrm{i}}(t)$ the signature of the scattered H-polarized pulse.

In view of the linearity and the time invariance of the configuration, we can write

$$E_0^{\mathrm{s}}(t) = S^E(t) \overset{(t)}{*} E_0^{\mathrm{i}}(t) \tag{28}$$

with $S^E(t)$ as the time-domain scattering coefficient of E-polarized waves, and

$$H_0^{\mathrm{s}}(t) = S^H(t) \overset{(t)}{*} H_0^{\mathrm{i}}(t) \tag{29}$$

with $S^H(t)$ as the time-domain scattering coefficient of H-polarized waves and where $\overset{(t)}{*}$ denotes time convolution.

Substitution of the field representations (24)–(29) in the boundary conditions (13) and (14) leads to expressions from which $S^E(t)$ and $S^H(t)$ can be determined. (Note that the continuity condition (13) is already satisfied by (24)–(29).) The most versatile way to carry out this procedure is via the use of the time Laplace transformation. To show the notation, we give the definition applied to the pulse signatures of the incident waves

$$\{\hat{E}_0^{\mathrm{i}}, \hat{H}_0^{\mathrm{i}}\}(s) = \int_{t=0}^{\infty} \exp(-st)\{E_0^{\mathrm{i}}, H_0^{\mathrm{i}}\}(t)\mathrm{d}t \quad \text{for } s \in \mathbb{C},\ \mathrm{Re}(s) > 0. \tag{30}$$

Under this transformation, the operator $\overset{(t)}{*}$ acting on two time functions transforms into the product of their time Laplace transforms and time differentiation transforms into a multiplication by the factor of s.

Substitution of the time Laplace transforms of the field representations (24)–(29) into the time Laplace transforms of the boundary conditions (13) and (14) leads to the following.

C. E-Polarized Field

$$\hat{S}^E(s) = -1 + \frac{2\alpha_z Y_0}{2\alpha_z Y_0 + G_{\mathrm{L}} + sC_{\mathrm{L}}} \tag{31}$$

and

D. H-Polarized Field

$$\hat{S}^H(s) = -1 + \frac{2}{2 + \alpha_z Z_0(G_{\mathrm{L}} + sC_{\mathrm{L}})}. \tag{32}$$

The corresponding time-domain expressions are:

E. E-Polarized Field

$$S^E(t) = -\delta(t) + T^E \exp(-\beta^E t) H(t) \tag{33}$$

with

$$T^E = 2\alpha_z \frac{Y_0}{C_\mathrm{L}} \tag{34}$$

$$\beta^E = T^E + \frac{G_\mathrm{L}}{C_\mathrm{L}} \tag{35}$$

and

F. H-Polarized Field

$$S^H(t) = -\delta(t) + T^H \exp(-\beta^H t) H(t) \tag{36}$$

with

$$T^H = \frac{2}{\alpha_z Z_0 C_\mathrm{L}} \tag{37}$$

$$\beta^H = T^H + \frac{G_\mathrm{L}}{C_\mathrm{L}} \tag{38}$$

in which $\delta(t)$ is the Dirac delta distribution and $H(t)$ is the Heaviside unit step function. (Note that $\beta^E > T^E$ and $\beta^H > T^H$.)

For no contrast in the layer ($G_\mathrm{L} = 0$ and $C_\mathrm{L} = 0$), both $S^E(t) = 0$ and $S^H(t) = 0$, as it should (no scattering). In the special case of conductive contrast only ($G_\mathrm{L} \neq 0$, $C_\mathrm{L} = 0$), $S^E(t) = -[G_\mathrm{L}/(2\alpha_z Y_0 + G_\mathrm{L})]\delta(t)$ and $S^H(t) = -[\alpha_z Z_0 G_\mathrm{L}/(2 + \alpha_z Z_0 G_\mathrm{L})]\delta(t)$.

IV. Numerical Results

In this section we present some numerical results for two types of pulse shape of the incident wave: the rectangular pulse and the trapezoidal pulse. The rectangular pulse, with its infinitely steep flanges can serve as a truly critical benchmark in the analysis of pulsed wave propagation problems with the aid of all sorts of time-domain computational electromagnetics software (either commercially available or at an experimental stage of development). The trapezoidal pulse is the standard pulse in the analysis of electromagnetic field and waves behavior in digital communications, electromagnetic compatibility (EMC) and the performance of nano-electronic semiconductor devices. The governing electromagnetic parameters in the reflection/transmission structure are: the *layer conductance ratio*

$$\eta_\mathrm{L} = \frac{G_\mathrm{L}}{Y_0} = G_\mathrm{L} Z_0 \tag{39}$$

the *layer admittance time constant*

$$\tau_\mathrm{L} = \frac{C_\mathrm{L}}{G_\mathrm{L}}. \tag{40}$$

The incident wave is characterized by its *direction of incidence* α_x (projection of the unit vector along the direction of propagation on the plane of the scattering layer), its *pulse time width* t_w for the *rectangular pulse* and its *pulse rise time* t_r, *pulse time width* t_w and *pulse fall time* t_f of the *trapezoidal pulse*.

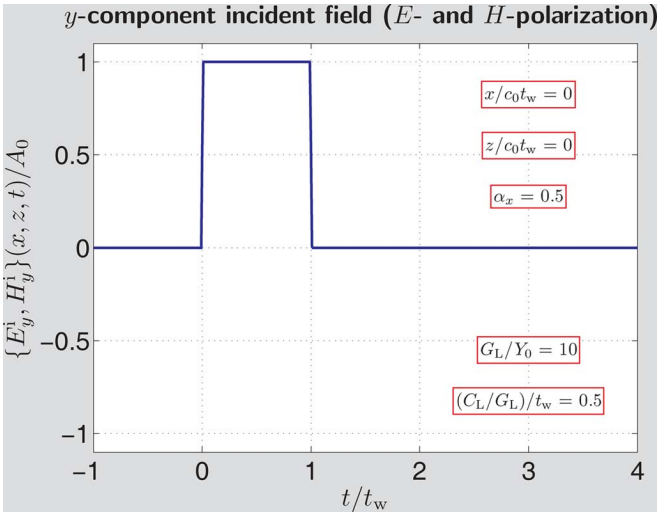

Fig. 3. Incident plane wave of rectangular pulse shape (E-polarization and H-polarization).

To arrive at the results, Matlab7.1 routines have been composed that, after properly editing the input data, generate a variety of field time snaps at a specified location, Matlab "images" (2D color density plots) of the field distribution in space at successive time instants (animation) and Matlab "quivers" (2D vector plots) of the Poynting vector distribution in space at successive time instants (animation).[2] Since the layered structure only influences the electric behavior of the configuration, the results for E-polarized waves differ essentially from the ones for H-polarized waves. Also, the field behavior in front of the layer is considerably different from the one behind it. This difference is most pronounced in the region of width $c_0 t_\mathrm{w}$ in front of the layer. For the case of the incident wave with *rectangular* pulse shape, we take, for the two types of polarization

$$\{E_0^\mathrm{i}, H_0^\mathrm{i}\} = A_0[H(t) - H(t - t_\mathrm{w})] \tag{41}$$

where A_0 is the *pulse amplitude* and $H(t)$ is the unit step function ($H(t) = \{0, 1\}$ for $\{t < 0, t \geq 0\}$) (Fig. 3). Here, the fundamental constituent to the pulse shape of the scattered wave is its unit step response, which we denote, for the two types of polarization, by $\{e^\mathrm{s}|_\mathrm{step}, h^\mathrm{s}|_\mathrm{step}\}(t)$. Obviously, in terms of this response

$$\{E_0^\mathrm{s}, H_0^\mathrm{s}(t)\} = A_0[\{e^\mathrm{s}|_\mathrm{step}, h^\mathrm{s}|_\mathrm{step}\}(t) - \{e^\mathrm{s}|_\mathrm{step}, h^\mathrm{s}|_\mathrm{step}\}(t - t_\mathrm{w})]. \tag{42}$$

For the case of the incident wave with *trapezoidal* pulse shape, we take, for the two types of polarization

$$\begin{aligned}\{E_0^\mathrm{i}, H_0^\mathrm{i}\} = A_0[&t_\mathrm{r}^{-1}\mathrm{ramp}(t) - t_\mathrm{r}^{-1}\mathrm{ramp}(t - t_\mathrm{r}) \\ &- t_\mathrm{f}^{-1}\mathrm{ramp}\left(t - \frac{t_\mathrm{r}}{2} - t_\mathrm{w} + \frac{t_\mathrm{f}}{2}\right) \\ &+ t_\mathrm{f}^{-1}\mathrm{ramp}\left(t - \frac{t_\mathrm{r}}{2} - t_\mathrm{w} - \frac{t_\mathrm{f}}{2}\right)\end{aligned} \tag{43}$$

[2]A copy of the routines is available upon request from the first author at: a.t.dehoop@tudelft.nl

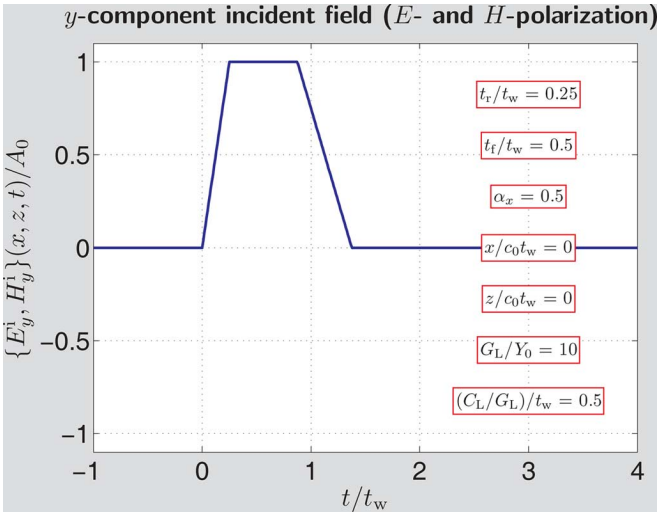

Fig. 4. Incident plane wave of trapezoidal pulse shape (E-polarization and H-polarization).

where A_0 is the *pulse amplitude* and $\mathrm{ramp}(t)$ is the unit ramp function ($\mathrm{ramp}(t) = \{0, t\}$ for $\{t < 0, t \geq 0\}$ (Fig. 4). Here, the fundamental constituent to the pulse shape of the scattered wave is its unit ramp response, which we denote, for the two types of polarization, by $\{e^{\mathrm{s}}|_{\mathrm{ramp}}, h^{\mathrm{s}}|_{\mathrm{ramp}}\}(t)$. Obviously, in terms of this response,

$$\begin{aligned}\{E_0^{\mathrm{s}}, H_0^{\mathrm{s}}\}(t) = A_0 \Big[& t_{\mathrm{r}}^{-1}\{e^{\mathrm{s}}|_{\mathrm{ramp}}, h^{\mathrm{s}}|_{\mathrm{ramp}}\}(t) \\ & - t_{\mathrm{r}}^{-1}\{e^{\mathrm{s}}|_{\mathrm{ramp}}, h^{\mathrm{s}}|_{\mathrm{ramp}}\}(t - t_{\mathrm{r}}) \\ & - t_{\mathrm{f}}^{-1}\{e^{\mathrm{s}}|_{\mathrm{ramp}}, h^{\mathrm{s}}|_{\mathrm{ramp}}\}\left(t - \frac{t_{\mathrm{r}}}{2} - t_{\mathrm{w}} + \frac{t_{\mathrm{f}}}{2}\right) \\ & + t_{\mathrm{f}}^{-1}\{e^{\mathrm{s}}|_{\mathrm{ramp}}, h^{\mathrm{s}}|_{\mathrm{ramp}}\}\left(t - \frac{t_{\mathrm{r}}}{2} - t_{\mathrm{w}} - \frac{t_{\mathrm{f}}}{2}\right)\Big].\end{aligned} \tag{44}$$

A. Unit Step Response (E-Polarization)

On account of the results of Section III, the time Laplace transform of $e^{\mathrm{s}}|_{\mathrm{step}}(t)$ follows, together with s^{-1} as the time Laplace transform of $H(t)$, as

$$\hat{e}^{\mathrm{s}}|_{\mathrm{step}}(s) = \hat{S}^E(s)\frac{1}{s} = \left(-1 + \frac{T^E}{s + \beta^E}\right)\frac{1}{s} \tag{45}$$

from which the time-domain pulse shape follows as

$$e^{\mathrm{s}}|_{\mathrm{step}}(t) = -H(t) + \frac{T^E}{\beta^E}\left[1 - \exp(-\beta^E t)\right] H(t) \tag{46}$$

in which [cf. (34) and (35)]

$$\frac{T^E}{\beta^E} = \frac{2\alpha_z}{2\alpha_z + \eta_{\mathrm{L}}} \tag{47}$$

$$\beta^E = \frac{\frac{2\alpha_z}{\eta_{\mathrm{L}}} + 1}{\tau_{\mathrm{L}}}. \tag{48}$$

B. Unit Step Response (H-Polarization)

On account of the results of Section III, the time Laplace transform of $h^{\mathrm{s}}|_{\mathrm{step}}(t)$ is

$$\hat{h}^{\mathrm{s}}|_{\mathrm{step}}(s) = \hat{S}^H(s)\frac{1}{s} = \left(-1 + \frac{T^H}{s + \beta^H}\right)\frac{1}{s} \tag{49}$$

from which the time-domain pulse shape follows as

$$h^{\mathrm{s}}|_{\mathrm{step}}(t) = -H(t) + \frac{T^H}{\beta^H}\left[1 - \exp(-\beta^H t)\right] H(t) \tag{50}$$

in which [cf. (37) and (38)]

$$\frac{T^H}{\beta^H} = \frac{2}{2 + \alpha_z\eta_{\mathrm{L}}} \tag{51}$$

$$\beta^H = \frac{\frac{2}{\alpha_z\eta_{\mathrm{L}}} + 1}{\tau_{\mathrm{L}}}. \tag{52}$$

C. Unit Ramp Response (E-Polarization)

On account of the results of Section III, the time Laplace transform of $e^{\mathrm{s}}|_{\mathrm{ramp}}(t)$ follows, together with s^{-2} as the time Laplace transform of $\mathrm{ramp}(t)$, as

$$\hat{e}^{\mathrm{s}}|_{\mathrm{ramp}}(s) = \hat{S}^E(s)\frac{1}{s^2} = \left(-1 + \frac{T^E}{s + \beta^E}\right)\frac{1}{s^2} \tag{53}$$

from which the time-domain pulse shape follows as

$$\begin{aligned}e^{\mathrm{s}}|_{\mathrm{ramp}}(t) = & \left(-1 + \frac{T^E}{\beta^E}\right)\mathrm{ramp}(t) \\ & - \frac{T^E}{(\beta^E)^2}\left[1 - \exp(-\beta^E t)\right] H(t).\end{aligned} \tag{54}$$

D. Unit Ramp Response (H-Polarization)

On account of the results of Section III, the time Laplace transform of $h^{\mathrm{s}}|_{\mathrm{ramp}}(t)$ follows, together with s^{-2} as the time Laplace transform of $\mathrm{ramp}(t)$, as

$$\hat{h}^{\mathrm{s}}|_{\mathrm{ramp}}(s) = \hat{S}^H(s)\frac{1}{s^2} = \left(-1 + \frac{T^H}{s + \beta^H}\right)\frac{1}{s^2} \tag{55}$$

from which the time-domain pulse shape follows as

$$\begin{aligned}h^{\mathrm{s}}|_{\mathrm{ramp}}(t) = & \left(-1 + \frac{T^H}{\beta^H}\right)\mathrm{ramp}(t) \\ & - \frac{T^H}{(\beta^H)^2}\left[1 - \exp(-\beta^H t)\right] H(t).\end{aligned} \tag{56}$$

From these results, the pulse shapes $\{E_0^{\mathrm{r}}, H_0^{\mathrm{r}}\}(t) = \{E_0^{\mathrm{s}}, H_0^{\mathrm{s}}\}(t)$ of the reflected wave in $\mathcal{D}^-$ and the pulse shapes $\{E_0^t, H_0^t\}(t) = \{E_0^{\mathrm{i}}, H_0^{\mathrm{i}}\}(t) + \{E_0^{\mathrm{s}}, H_0^{\mathrm{s}}\}(t)$ of the transmitted wave in $\mathcal{D}^+$ can be constructed. Figs. 5–10 show some results for an incident wave with rectangular pulse shape.

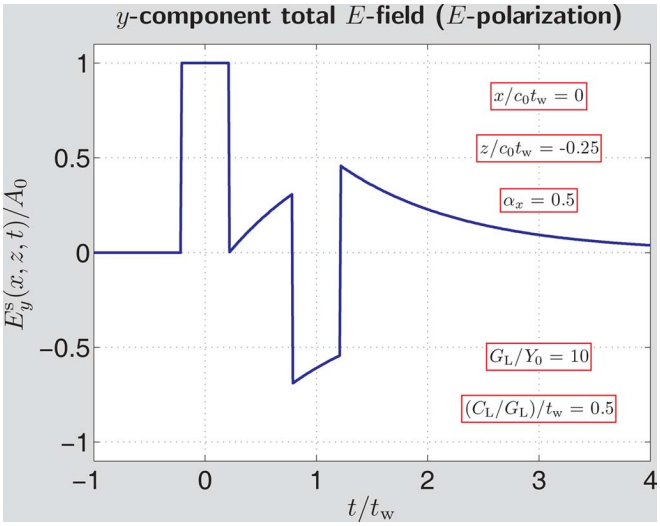

Fig. 5. Time snap in front of, and in the vicinity of, the scattering layer (E-polarization, rectangular incident pulse).

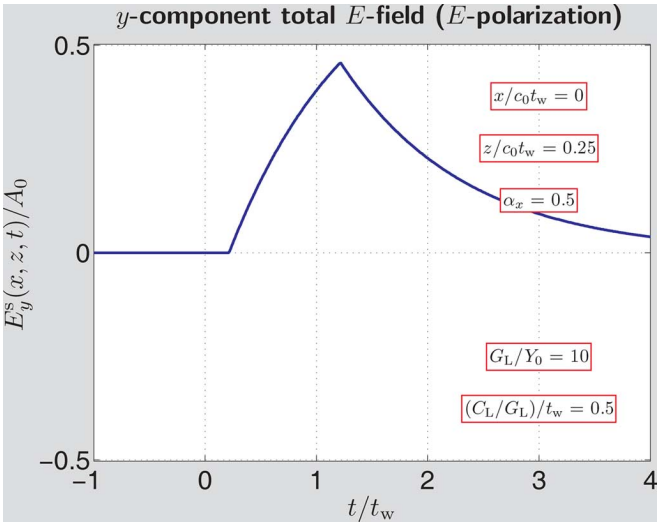

Fig. 6. Time snap behind, and in the vicinity of, the scattering layer (E-polarization, rectangular incident pulse).

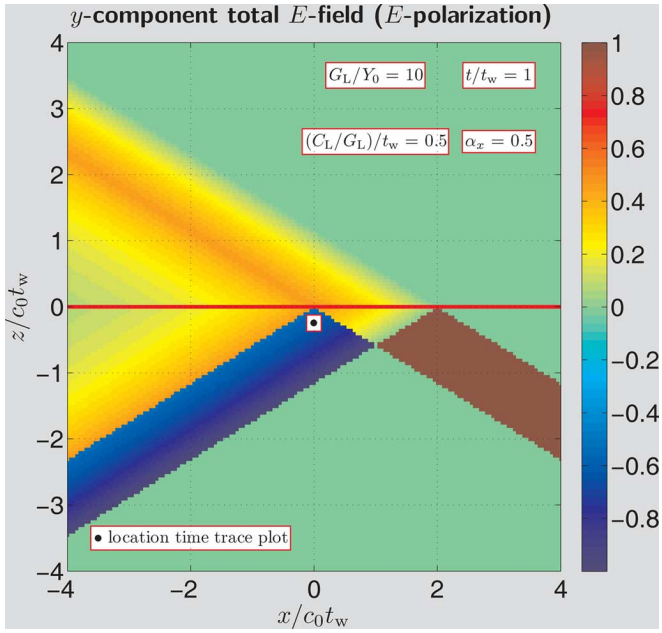

Fig. 7. Density plot in domain about the scattering layer (E-polarization, rectangular incident pulse). The indicated location of time plot traces applies to Figs. 5 and 8.

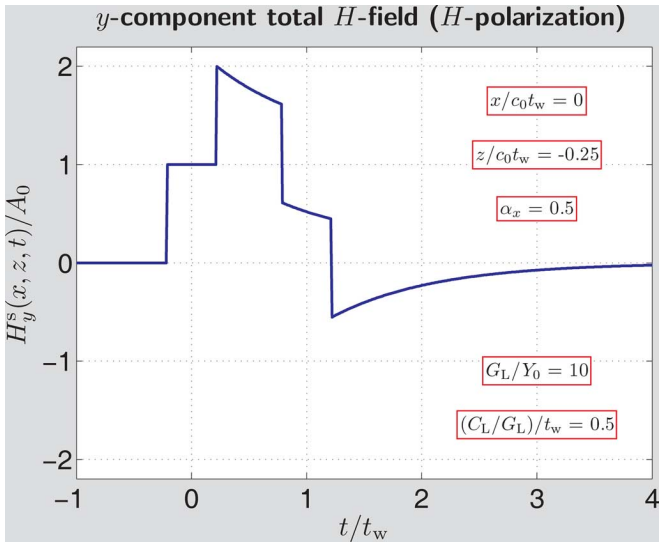

Fig. 8. Time snap in front of, and in the vicinity of, the scattering layer (H-polarization, rectangular incident pulse).

Figs. 11–16 show results for an incident wave with trapezoidal pulse shape. The figures indicate how drastically the pulse shapes can deviate from the one of the incident wave, as well as how different E-polarized field behave from H-polarized fields. The results clearly indicate the differences in response of E- *versus* H-polarized fields. This could be expected since the contrast properties of the thin sheet involve only electrical material parameters (conductivity and permittivity) and no magnetic material parameters. The differences in response imply, in particular, that the pulse shapes of arbitrarily polarized and obliquely incident waves undergo rather complicated changes upon their interaction with the thin-sheet configuration. In any communication system based on pulse operation this is a factor of importance. The results for the pulse of rectangular shape, with its infinitely steep flanges and zero pulse rise and fall times, illustrate to what non-zero pulse rise and fall times the reflection against and transmission across the thin sheet give rise, any non-zero pulse rise or fall time, in this case, being attributable to the presence of the configuration. The results for the pulse with trapezoidal shape have been included as this pulse shape is the standard pulse for analyzing the signal and field transfer in digital microelectronic devices and systems.

V. The Thin-Sheet, High-Contrast Boundary Condition in More Complex Configurations

In highly complex configurations, the thin-sheet, high-contrast boundary condition (12) can be implemented in any type of mesh-conforming spatial discretization as used in finite-difference and finite-element methods for solving Maxwell's equations in the time domain. Configurations containing one or more

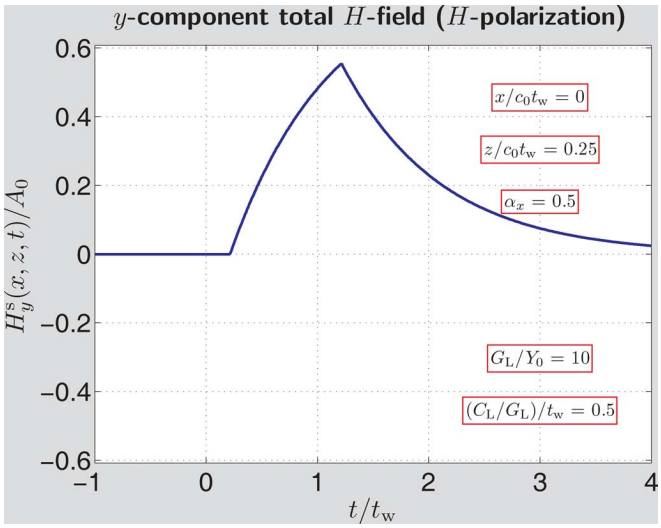

Fig. 9. Time snap behind, and in the vicinity of, the scattering layer (H-polarization, rectangular incident pulse).

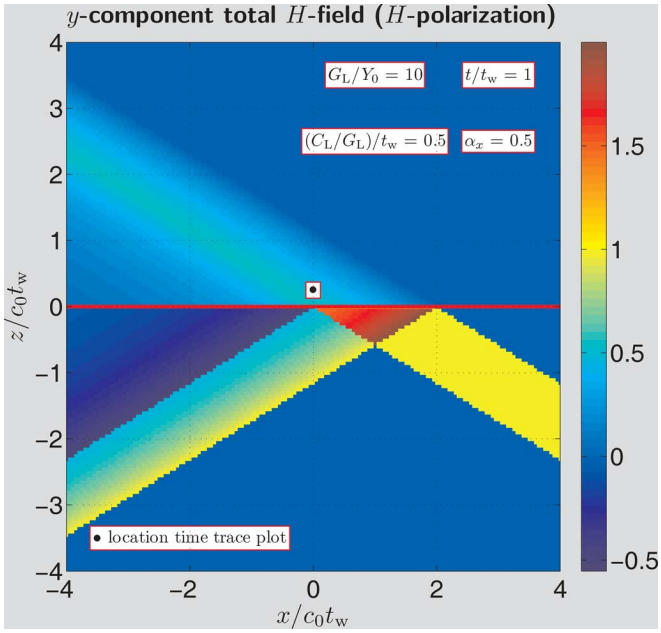

Fig. 10. Density plot in domain about the scattering layer (H-polarization, rectangular incident pulse). The indicated location of time trace plot applies to Figs. 6 and 9.

thin-sheet, high-contrast disks of finite planar supports and embedded in a homogeneous, isotropic embedding, can advantageously be handled via an integral-equation formulation. We illustrate the relevant procedure by considering the scattering of an arbitrary incident field $\{\boldsymbol{E}^{\mathrm{i}}, \boldsymbol{H}^{\mathrm{i}}\}(\boldsymbol{r}, t)$ by the disk specified by (1). The contrast sheet electric current density $\boldsymbol{J}^{\mathrm{s}}_{\mathrm{sheet}}$ generates the scattered field $\{\boldsymbol{E}^{\mathrm{s}}, \boldsymbol{H}^{\mathrm{s}}\}(\boldsymbol{r}, t)$. The electric field of the latter is related to $\boldsymbol{J}^{\mathrm{s}}_{\mathrm{sheet}}$ via \

$$[\boldsymbol{E}^{\mathrm{s}}(\boldsymbol{r},t)] = \int_{(x',y')\in\Sigma} \left[G^{E,J}\right](\boldsymbol{r};x',y',0;t) \overset{(t)}{*} [\boldsymbol{J}^{\mathrm{s}}_{\mathrm{sheet}}(x',y',t)]\,\mathrm{d}x'\mathrm{d}y' \quad \text{for } \boldsymbol{r}\in\mathbb{R}^3 \text{and } t\in\mathbb{R} \tag{57}$$

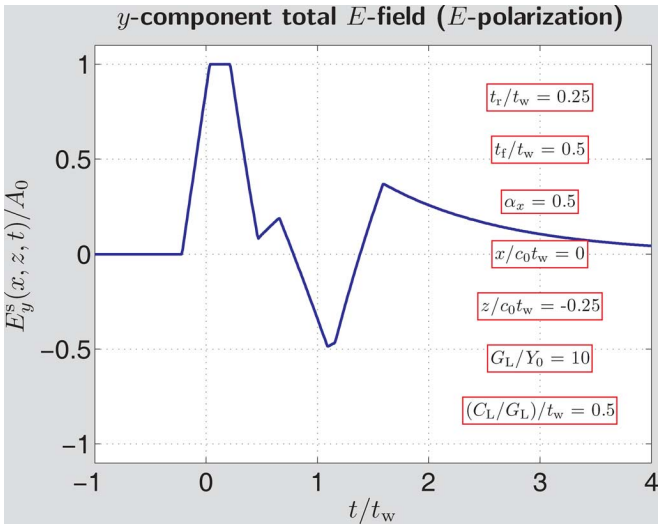

Fig. 11. Time snap in front of, and in the vicinity of, the scattering layer (E-polarization, trapezoidal incident pulse). The indicated location of time trace plot applies to Figs. 11 and 14.

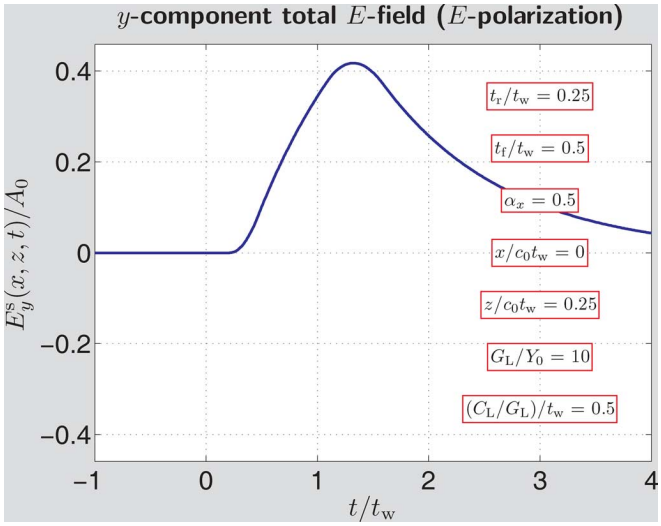

Fig. 12. Time snap behind, and in the vicinity of, the scattering layer (E-polarization, trapezoidal incident pulse).

in which $[\boldsymbol{E}^{\mathrm{s}}]$ is the 1×3 matrix of the Cartesian components of the scattered electric field, $\left[G^{E,J}\right]$ is the 3×3 matrix of the Cartesian components of the electric-field/electric-current Green's tensor of rank two [4, pp. 732–733] and $[\boldsymbol{J}^{\mathrm{s}}_{\mathrm{sheet}}]$ is the 1×3 matrix of the Cartesian components of the contrast sheet electric current density (with zero z-component). Taking (57) for $z = 0$ and $(x,y)\in\Sigma$ and substituting the result in the right-hand side of [cf. (12)]

$$J^{\mathrm{s}}_{\mathrm{sheet};x,y}(x,y,t) = (G_{\mathrm{L}} + C_{\mathrm{L}}\partial_t)(E^{\mathrm{i}}_{x,y}(x,y,0,t) + E^{\mathrm{s}}_{x,y}(x,y,0,t)) \quad \text{for } (x,y)\in\Sigma \text{ and all } t\in\mathbb{R} \tag{58}$$

we end up with integral equations for $J^{\mathrm{s}}_{\mathrm{sheet};x}$ and $J^{\mathrm{s}}_{\mathrm{sheet};y}$ that can be solved with standard numerical methods such as can be found in [17].

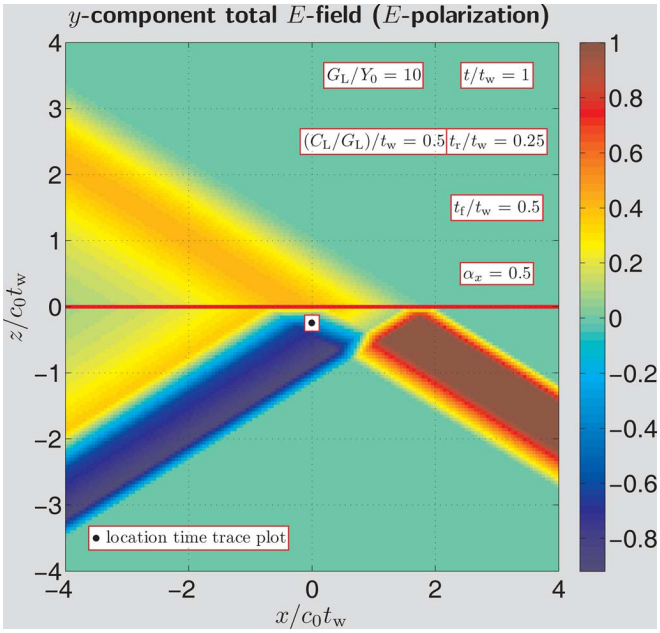

Fig. 13. Density plot in domain about the scattering layer (E-polarization, trapezoidal incident pulse). The indicated location of time trace plot applies to Figs. 11 and 14.

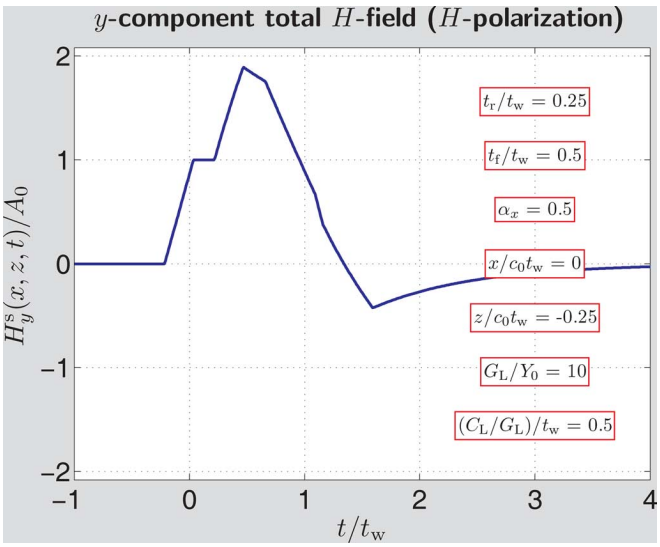

Fig. 14. Time snap in front of, and in the vicinity of, the scattering layer (H-polarization, trapezoidal incident pulse).

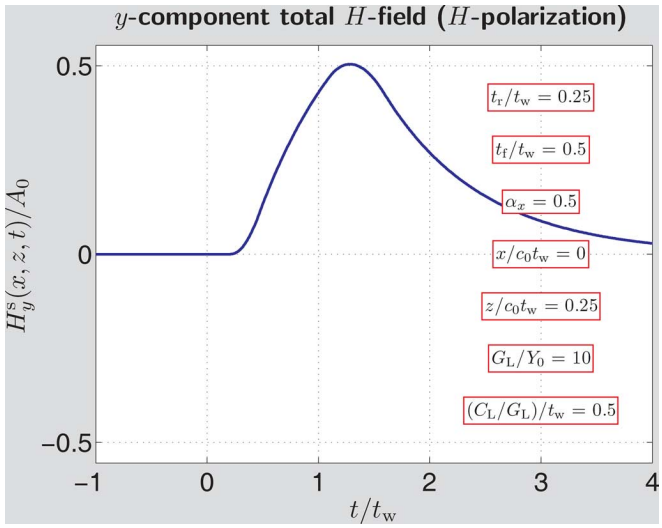

Fig. 15. Time snap behind, and in the vicinity of, the scattering layer (H-polarization, trapezoidal incident pulse).

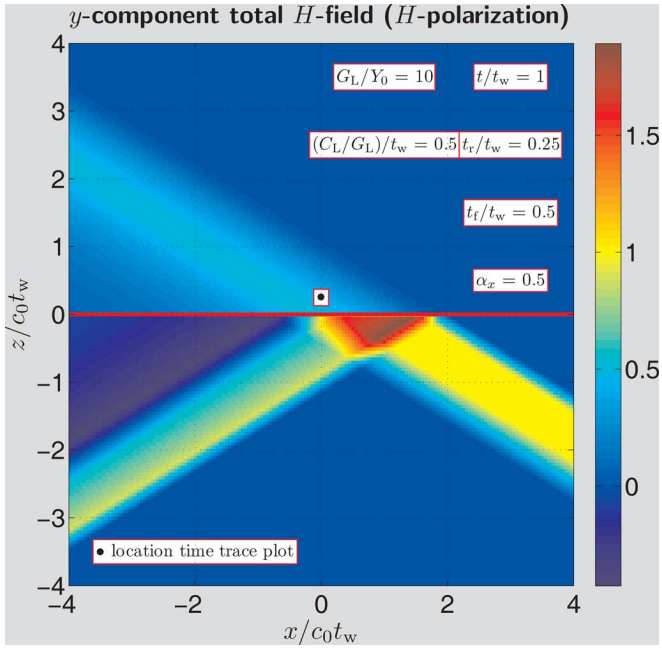

Fig. 16. Density plot in domain about the scattering layer (H-polarization, trapezoidal incident pulse). The indicated location of time trace plot applies to Figs. 12 and 15.

VI. Conclusion

An approximate method is proposed that models the interaction of an incident, pulsed, electromagnetic field with a thin, high-contrast, finely layered structure via a thin-sheet boundary condition that expresses the in-plane conduction and contrast electric polarization currents in the structure in terms of the exciting incident field. The boundary condition relates the jump in the tangential component of the scattered magnetic field strength across the layer in terms of the (continuous) tangential component of the electric field strength in the layer. In the pertaining layer admittance coefficient, the integrated values of the conductance and the contrast permittivity profiles across the layer occur. The model is applied to the scattering of an incident plane wave with pulsed time signature by a layer of infinite extent. Expressions for the pulse shapes of the reflected and transmitted fields are obtained. In them, the layer properties and the direction of incidence and state of polarization of the incident wave occur as parameters. Numerical results for incident waves with rectangular and trapezoidal pulse shapes illustrate how the thin-layer structure change the pulse shapes of the total field in front of and behind the scattering layer.

The use of the thin-sheet, high-contrast boundary condition in the computational analysis in more complex configurations is briefly indicated.

ACKNOWLEDGMENT

The authors would like to thank A. Deutsch, B. J. Rubin, and J. D. Morsey at IBM T.J. Watson Research Center for many helpful discussions. The authors also would like to thank the reviewers for their careful reading of the manuscript, their constructive criticism and their suggestions for improvement of the paper.

REFERENCES

[1] I. T. Chiang and W. C. Chew, "Thin dielectric sheet simulation by surface integral equation using modified RWG and pulse basis," *IEEE Trans. Antennas Propag.*, vol. 54, no. 7, pp. 1927–1934, Jul. 2006.

[2] R. F. Harrington and J. R. Mautz, "An impedance sheet approximation for thin dielectric shells," *IEEE Trans. Antennas Propag.*, vol. 23, pp. 531–534, Jul. 1975.

[3] I. S. Koh and K. Sarabandi, "A new approximate solution for scattering by thin dielectric disks of arbitrary size and shape," *IEEE Trans. Antennas Propag.*, vol. 53, no. 6, pp. 1920–1926, Jun. 2005.

[4] A. T. De Hoop, *Handbook of Radiation and Scattering of Waves*. London: Academic Press, 1995.

[5] V. H. Rumsey, "The reaction concept in electromagentic theory," *The Physical Review*, vol. 94, pp. 1483–1491, Jun. 1954.

[6] R. F. Harrington, *Time-Harmonic Electromagnetic Fields*. New York: McGraw-Hill, 1960.

[7] R. E. Collin, *Field Theory of Guided Waves*, 2nd ed. New York: IEEE Press, 1991.

[8] T. B. E. Senior, "Approximate boundary conditions," *IEEE Trans. Antennas Propag.*, vol. 29, pp. 826–829, Sep. 1981.

[9] T. B. E. Senior and J. L. Volakis, *Approximate Boundary Conditions in Electromagnetics*. London: IET Press, 1995.

[10] M. Schoenberg and F. Muir, "A calculus for finely layered anisotropic media," *Geophysics*, vol. 54, no. 5, pp. 581–589, May 1989.

[11] J. M. Hovem, "Acoustic waves in finely layered media," *Geophysics*, vol. 60, no. 4, pp. 1217–1221, Jul.-Aug. 1995.

[12] V. Lomakin, B. Z. Steinberg, and E. Heyman, "Multi-resolution homogenization (MRH) for short pulse field and fault interrogation in complex laminates," in *Ultra-Wideband, Short-pulse Electromagnetics*. New York: Kluwer Academic/Plenum Publishers, 2003, vol. 6, pp. 203–214.

[13] C. J. Bouwkamp, "Diffraction theory," in *Reports on Progress Phys.*, 1954, vol. 17, pp. 35–100, 45.

[14] A. T. De Hoop, "A time-domain uniqueness theorem for electromagnetic wavefeld modeling in dispersive, anisotropic media," *URSI – Radio Sci. Bull.*, no. 305, pp. 17–21, Jun. 2003.

[15] J. Meixner, The Behavior of Electromagnetic Fields at Edges Institute of Mathematical Sciences New York University, New York, 1954, Rep. Nr. EM-72.

[16] A. E. Heins and S. Silver, "The edge conditions and field representation theorems in the theory of electromagnetic diffraction," in *Proc. Cambridge Philos. Society*, 1955, vol. 51, pp. 149–161.

[17] R. Mittra, "Integral equation methods for transient scattering," in *Transient Electromagnetic Fields*, L. B. Felsen, Ed. Berlin: Springer-Verlag, 1976, ch. 2.

Adrianus T. DeHoop (M'00) was born in Rotterdam, the Netherlands, on December 24, 1927. He received the M.Sc. degree in electrical engineering in 1950 and the Ph.D. degree in the technological sciences in 1958 from Delft University of Technology, Delft, The Netherlands, both with the highest distinction.

He served Delft University of Technology as an Assistant Professor from 1950 to 1957, Associate Professor from 1957 to 1960, and Full Professor in electromagnetic theory and applied mathematics from 1960 to 1996, and since 1996, he has been the Lorentz Chair Emeritus Professor in the Faculty of Electrical Engineering, Mathematics and Computer Science. In 1970, he founded the Laboratory of Electromagnetic Research at Delft University of Technology which has developed into a world-class center for electromagnetics. His research interests are in the broad area of wavefield modeling in acoustics, electromagnetics and elastodynamics. His interdisciplinary insights and methods in this field can be found in his *Handbook of Radiation and Scattering of Waves* (London, Academic Press, 1995), with wavefield reciprocity serving as one of the unifying principles governing direct and inverse scattering problems and wave propagation in complex (anisotropic and dispersive) media. From 1956 to 1957, he was a Research Assistant with the Institute of Geophysics, University of California at Los Angeles, where he pioneered a modification of the Cagniard technique for calculating impulsive wave propagation in layered media, later to be known as the "Cagniard-De-Hoop technique." On a regular basis, since 1982, he a Visiting Scientist with Schlumberger-Doll Research, Ridgefield, CT (presently at Cambridge, MA), where he contributes to research on geophysical applications of acoustic, electromagnetic and elastodynamic waves. Recently, he is exploring a method for computing pulsed electromagnetic fields in strongly heterogeneous media with application to (micro- or nano-scale) integrated circuits.

Dr. De Hoop is a Member of the Royal Netherlands Academy of Arts and Sciences and a Foreign Member of the Royal Flemish Academy of Belgium for Science and Arts. He holds an Honorary Doctorate in the Applied Sciences from Ghent University, Belgium (1981). Grants from the "Stichting Fund for Science, Technology and Research" (founded by Schlumberger Limited) supported his research at Delft University of Technology. He was awarded the 1989 Research Medal of the Royal Institute of Engineers in The Netherlands, the IEEE 2001 Heinrich Hertz Gold Research Medal, and the 2002 URSI (International Scientific Radio Union) Balthasar van der Pol Gold Research Medal. In 2003, Her Majesty the Queen of The Netherlands decorated him "Knight in the Order of the Netherlands Lion."

Lijun Liang (M'05) received the B.S. degree in electrical engineering from Beijing University of Aeronautics and Astronautics, Beijing, China, in 1993, the M.S. degree from Tsinghua University, China, in 1996, and the Ph.D. degree from the University of Illinois at Urbana-Champaign, in 2004.

From 1996 to 1999, he was an Application Engineer with Hewlett-Packard. Since 2004, he has been a Postdoctoral Researcher and Research Staff Member at the IBM T.J. Watson Research Center. His research interests focus on computational electromagnetics, signal integrity, fast numerical algorithms, parallel algorithms, EMC, and antennas, etc.

Dr. Liang received the IEEE MTT Graduate Fellowship Award in 2003 and the Y.T. Lo Outstanding Research Award in 2004. He is a Sigma Xi Associate Member. He also serves as a reviewer of the IEEE TRANSACTIONS ON ANTENNA AND PROPAGATION and the IEEE TRANSACTIONS ON ADVANCED PACKAGING.